Available online at www.sciencedirect.com
SCIENCE DIRECT®
PERGAMON
Deep-Sea Research I 50 (2003) 987–1003
DEEP-SEA RESEARCH PART I
www.elsevier.com/locate/dsr

The generation of internal tides at abrupt topography

Louis St. Laurent[a,*], Steven Stringer[b], Chris Garrett[c], Dominique Perrault-Joncas[d]

[a] Department of Oceanography, Florida State University, Tallahassee, FL 32306, USA
[b] School of Earth and Ocean Sciences, University of Victoria, Victoria, BC, Canada
[c] Department of Physics and Astronomy, University of Victoria, Victoria, BC, Canada
[d] Department of Physics, McGill University, Montreal, QC, Canada

Received 23 July 2002; received in revised form 2 April 2003; accepted 2 April 2003

Abstract

Internal tide generation is examined for a knife-edge ridge and an abrupt step. The energy flux from a knife-edge ridge with a height much less than the water depth is shown to be twice that from a Witch of Agnesi ridge with the same height but a small slope. In contrast, the energy flux from an abrupt step with an infinitesimal depth change compared to the water depth is the same as from a small slope with the same depth change. For larger topographic heights in both cases, the energy flux from the abrupt topography can significantly exceed that from gentle topography. The energy flux generated at a top-hat ridge and top-hat trench is also calculated. A top-hat ridge generates more energy flux than a knife edge of equivalent height, though the increase is large only for ridges whose height is small compared to the total depth. Additionally, the energy flux produced by a top-hat ridge is found to be rather insensitive to the ridge width. In contrast, the energy flux generated at a top-hat trench is strongly dependent on width. A knife-edge ridge of moderate height has much of its energy flux in mode 1. For a height to depth ratio comparable to that of the Hawaiian Ridge this fraction is 75%, consistent with observations. We also show that energy flux estimates based on representing general topography as a number of independent steps are flawed.

1. Introduction

In the stratified ocean, internal tides are generated at regions where the barotropic tidal current encounters variations in bottom topography. The problem for the wave response involves the solution to the momentum, continuity, and buoyancy equations satisfying the surface ($z = 0$) and bottom ($z = -H + h(x, y)$) boundary conditions

$$w(0) = 0, \quad w(-H + h) = \mathbf{U} \cdot \nabla \mathrm{h} + \mathbf{u} \cdot \nabla \mathrm{h}. \qquad (1)$$

Here, $h(x, y)$ is the bottom topography relative to a deep constant-depth level $z = -H$, $\mathbf{U}$ is the barotropic tidal velocity for the region of depth H, and $\mathbf{u}(\mathrm{x}, \mathrm{y}, \mathrm{z}, \mathrm{t})$ and $w(x, y, z, t)$ are the lateral and vertical components of the baroclinic wave response. These waves obey the conventional dispersion relation of internal waves which can be expressed in terms of wave slope,

$$\alpha = \left|\frac{k}{m}\right| = \left(\frac{\omega^2 - f^2}{N^2 - \omega^2}\right)^{1/2}, \qquad (2)$$

where α is the wave slope, k and m are the lateral and vertical wavenumbers, and f and N are the

*Corresponding author.
E-mail address: lous@ocean.fsu.edu (L. St. Laurent).

0967-0637/03/$ - see front matter © 2003 Elsevier Ltd. All rights reserved.
doi:10.1016/S0967-0637(03)00096-7

inertial and buoyancy frequencies. We will take the tidal frequency ω satisfying the condition $f<\omega<N$ so that internal tides are freely radiating.

Several nondimensional parameters are needed to characterize the physical regime of wave generation. One parameter, kU_0/ω, measures the ratio of the tidal excursion length scale U_0/ω to the length scale of the topography k^{-1}. This parameter is discussed by Bell (1975) and others, and distinguishes a wave response dominated by the fundamental tidal frequency ($kU_0/\omega<1$) from a lee-wave response involving higher tidal harmonics ($kU_0/\omega>1$). A second parameter, $\delta=h_0/H$, measures the ratio of the topographic amplitude h_0 to the total depth H. A third parameter, $\varepsilon=s/\alpha$, measures the ratio of the maximum topographic slope $s=|\nabla h|$ to the ray slope given by (2). This parameter also distinguishes two regimes. In the case of $\varepsilon<1$, the topographic slopes are less steep than the radiated tidal beam, and internal wave generation is termed subcritical. In the case of $\varepsilon>1$, the topographic slopes exceed the steepness of the radiated beam and the internal wave generation is termed supercritical. The critical generation condition is met when the radiated tidal beam is aligned with the slope of the topography.

The subcritical generation of internal tides was first considered by Cox and Sandstrom (1962), Baines (1973), and Bell (1975). These studies examined subcritical topography in the limit of $\delta\ll1$ and $\varepsilon\ll1$, for which the bottom boundary condition can be linearized to $w(-H)=\mathbf{U}\cdot\nabla\mathrm{h}$. In this case, the internal tide generation problem can be solved for topography of arbitrary shape by Fourier decomposition. Later studies have examined the initial transient wave response, finite depth effects, depth varying stratification, and spatial variations in topography and tidal forcing (Hibiya, 1986; Khatiwala, 2003; Li, in press; Llewellyn Smith and Young, 2002; St. Laurent and Garrett, 2002). Of central interest in all studies is the tidal conversion rate F; the production of baroclinic energy as the barotropic tide responds to changes in topography. In the limit of small tidal excursion ($kU_0/\omega\ll1$), the conversion rate is equal to the energy flux away from the topography. Llewellyn Smith and Young (2002) show that the energy flux in the limits of $\varepsilon\ll1$ and $kU_0/\omega\ll1$ is

$$F_{\mathrm{linear}}=F_0H^{-2}\sum_{n=1}^{\infty}k_n\tilde{h}(k_n)\tilde{h}^{*}(k_n)\Delta k, \tag{3}$$

where $k_n=n\Delta k=\alpha n\pi/H$ denote the wavenumbers of the resonant modes and $\tilde{h}$ is the Fourier transform of the topography. Here,

$$F_0=\frac{1}{2\pi}\rho\frac{((N^2-\omega^2)(\omega^2-f^2))^{1/2}}{\omega}U_0^2H^2 \tag{4}$$

is a convenient metric for the energy flux amplitude, with the rest of (3) being nondimensional.

Internal tide generation at topography of finite steepness was considered by Baines (1982). In that study, ray tracing methods were developed to permit the full range of δ and ε. The integral equations derived by Baines (1982) are difficult to apply to arbitrary topography, and Baines did not examine the sensitivity of the conversion rate to the steepness of the topography. Using an approach similar to Baines, Craig (1987) specifically considered a continental slope of finite steepness, but only considered $\varepsilon\leqslant2$. Taking a different approach, St. Laurent and Garrett (2002) examined the first-order correction to linear theory estimates of energy flux for sinusoidal topography of subcritical steepness ($\varepsilon<1$), finding that

$$F=F_{\mathrm{linear}}\left(1+\frac{1}{4}\varepsilon^2+\cdots\right). \tag{5}$$

Full series expansions for the full corrections for sinusoidal and gaussian topographies were derived by Balmforth et al. (2002) for increasing steepness up to the critical condition ($\varepsilon=1$). They find increased levels of conversion at critical slopes, though the increase varies from only 14% for the gaussian ridge to 56% for the sinusoidal case.

Numerical simulations have allowed calculations of internal tide generation over the full variation of the steepness parameter. Studies by Khatiwala (2003) and Li (in press) also show increased energy flux production at critical topographies to levels comparable with those reported by Balmforth et al. (2002). Both Li (in press) and Khatiwala (2003) find a reduction in energy flux for supercritical sinusoidal topography. Khatiwala (2003) also explores isolated ridges, and finds that

the reduction in energy flux does not occur. He suggests that the downward propagating energy from supercritical sinusoidal topography will accumulate in valleys as trapped modes. While numerical simulations have provided some insights, the properties of internal tides generated at supercritical topography are still poorly understood.

In contrast to studies that explore wave generation for incremental increases in ε, models for generation at abrupt depth discontinuities ($\varepsilon = \infty$) have also been formulated. Rattray (1960) considered the first-mode baroclinic response to barotropic flow over shelf topography. Stigebrandt (1980) also considered a topographic step and examined the full spectrum of baroclinic modes. However, both of these studies focus on the coastal generation problem, where $\delta \simeq 1$. Past studies have not compared the energy flux production at abrupt topography with estimates made using linear theory.

In the present study, we examine the internal tide generation problem for a knife-edge ridge and a step. For the case of the knife-edge ridge (Section 2), we compare estimates of energy flux to linear theory estimates for the "Witch of Agnesi" ridge. For the case of the step (Section 3), we compare estimates of energy flux to linear theory estimates for a slope. In both cases, we examine the energy flux over the full range of δ, paying particular attention to the limit of $\delta \to 0$ applicable to small amplitude topography in the deep ocean. We extend the model for the step to examine energy flux generated by a top-hat ridge (Section 4.1) and a top-hat trench (Section 4.2). In Section 5, we discuss implications of these abrupt topography models. Internal tide energy flux for the Hawaiian Ridge is considered using the knife-edge ridge model in Section 5a. Finally, the model used by Sjöberg and Stigebrandt (1992) and Gustafsson (2001), in which arbitrary topography is represented as a number of independent steps, is examined in Section 5b. Conclusions are presented in Section 6.

2. Internal tide generation at a knife-edge ridge

We consider a knife-edge (zero width) ridge of height h_0 at $x = 0$ in an ocean of uniform depth H (Fig. 1). A barotropic tidal current is given by $U(t) = U_0 \cos \omega t$, taken perpendicular to the ridge. Previous studies by Larsen (1969) and Robinson (1969) have examined the scattering of waves, rather than wave generation, from a knife-edge ridge. While their solutions could be adapted to the barotropic to baroclinic conversion of the tide, we will use a straightforward approach based on matching conditions for the modal solutions:

$$u_1 = U_0 \sum_{n=1}^{\infty} a_n \cos\left(\frac{n\pi z}{H}\right) \cos\left(k_n x + \omega t\right),$$

$$u_2 = U_0 \sum_{n=1}^{\infty} b_n \cos\left(\frac{n\pi z}{H}\right) \cos\left(-k_n x + \omega t\right), \qquad (6)$$

$$w_1 = \alpha U_0 \sum_{n=1}^{\infty} a_n \sin\left(\frac{n\pi z}{H}\right) \sin\left(k_n x + \omega t\right),$$

$$w_2 = -\alpha U_0 \sum_{n=1}^{\infty} b_n \sin\left(\frac{n\pi z}{H}\right) \sin\left(-k_n x + \omega t\right), \qquad (7)$$

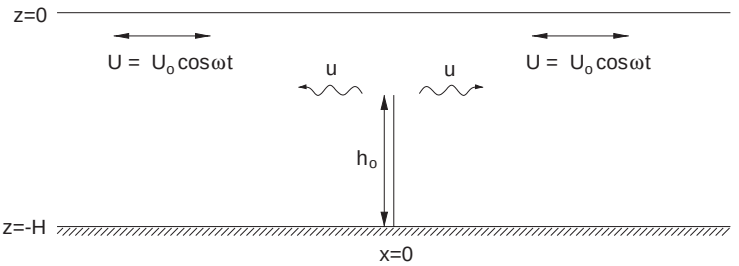

Fig. 1. Sketch showing a knife-edge ridge of height h_0 in an ocean of depth H. The barotropic tidal current and baroclinic response are denoted by U and u, respectively.

where a_n and b_n are the nondimensional coefficients of the modal series, $n\pi/H$ are vertical wavenumbers, and k_n are the horizontal wavenumbers given by (2) as $k_n = \alpha n\pi/H$. The subscripts 1 and 2 denote the baroclinic response on the $x<0$ and $x>0$ sides of the ridge, respectively. Here, the modal forms have been chosen to satisfy the boundary condition $w = 0$ at $z = 0$ and $z = -H$. The modal coefficients are obtained through matching conditions at $x = 0$,

$$w_1 = w_2, \quad -H + h_0 \leqslant z \leqslant 0, \tag{8}$$

$$u_1 + U = u_2 + U, \quad -H + h_0 \leqslant z \leqslant 0, \tag{9}$$

$$u_1 + U = 0, \quad -H \leqslant z < -H + h_0, \tag{10}$$

$$u_2 + U = 0, \quad -H \leqslant z < -H + h_0. \tag{11}$$

Relations (9)–(11) can be combined to show

$$\sum_{n=1}^{\infty} a_n \cos\frac{n\pi z}{H} = \sum_{n=1}^{\infty} b_n \cos\frac{n\pi z}{H}, \quad -H \leqslant z \leqslant 0. \tag{12}$$

Through the orthogonality of cosines, (12) implies $a_n = b_n$, a result which is also implied by the symmetry of the topography. This allows us to write all the matching conditions as two statements,

$$\sum_{n=1}^{\infty} a_n \sin\frac{n\pi z}{H} = 0, \quad -H + h_0 \leqslant z \leqslant 0, \tag{13}$$

$$\sum_{n=1}^{\infty} a_n \cos\frac{n\pi z}{H} = -1, \quad -H \leqslant z < -H + h_0. \tag{14}$$

The coefficients a_n can now be determined by a Fourier series expansion of the terms in (13) and (14). Multiplying by $\cos m\pi z/H$ and vertically integrating gives

$$\sum_{n=1}^{\infty} a_n \left(\int_{-H}^{-H+h_0} \cos\frac{n\pi z}{H}\cos\frac{m\pi z}{H}\,\mathrm{d}z + \int_{-H+h_0}^{0} \sin\frac{n\pi z}{H}\cos\frac{m\pi z}{H}\,\mathrm{d}z \right) = -\int_{-H}^{-H+h_0} \cos\frac{m\pi z}{H}\,\mathrm{d}z. \tag{15}$$

In practice, the summation in (15) is done over a finite number of modes, $n = 1, 2, \ldots, N$. Thus, for any integer choice of m, (15) gives an equation with N unknown a_n coefficients. A coupled set of N equations in N unknowns can be produced by taking $m = 0, 1, 2, \ldots, N-1$. These can be written in matrix form as

$$A_{mn} a_n = c_m, \tag{16}$$

where

$$A_{mn} = \frac{n \sin n\pi(1-\delta)\cos m\pi(1-\delta) - m\cos n\pi(1-\delta)\sin m\pi(1-\delta)}{(m^2-n^2)} + \frac{n - n\cos n\pi(1-\delta)\cos m\pi(1-\delta) - m\sin n\pi(1-\delta)\sin m\pi(1-\delta)}{(m^2-n^2)} \tag{17}$$

and

$$c_m = \frac{\sin m\pi(1-\delta)}{m}. \tag{18}$$

A_{mn} is singular when $m = n$, so those elements are replaced with those found by re-evaluating the integrals on the left-hand side of Eq. (15) after setting $m = n$, giving

$$A_{nn} = \frac{n\pi\delta - \sin n\pi(1-\delta)\cos n\pi(1-\delta) - \sin^2 n\pi(1-\delta)}{2n}. \tag{19}$$

Also, c_m is singular at $m = 0$. This element is replaced by setting $m = 0$ in the integral on the right-hand side of (15), yielding

$$c_0 = -\pi\delta. \tag{20}$$

The matrix problem (16) has been solved for 2000 baroclinic modes. The cosine expansion was also done for 2000 terms, $m = 0, 1, 2, \ldots, 1999$. This gives a square matrix for A_{mn}, and the coefficients a_n are given by the matrix inversion

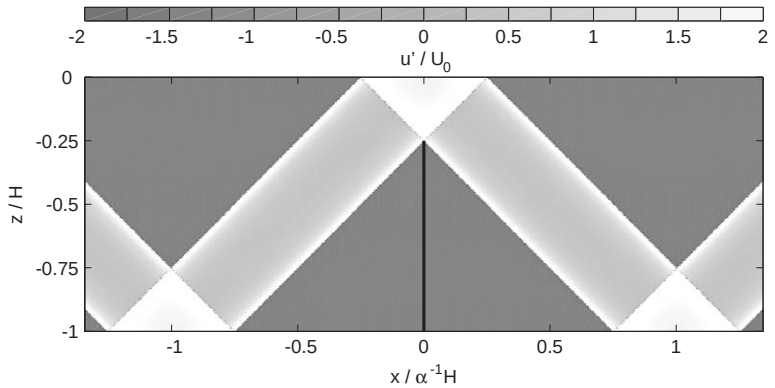

Fig. 2. A snapshot of instantaneous baroclinic velocity (u_1 and u_2 at $\omega t = 0, 2\pi, 4\pi, \ldots$, from (6)) normalized by the barotropic current amplitude, for the knife-edge ridge with $\delta = 0.75$. The ridge at $x = 0$ is shown, and the distance coordinate is normalized by $\alpha^{-1}H$. Dark gray shading indicates regions where $u = -U_0$.

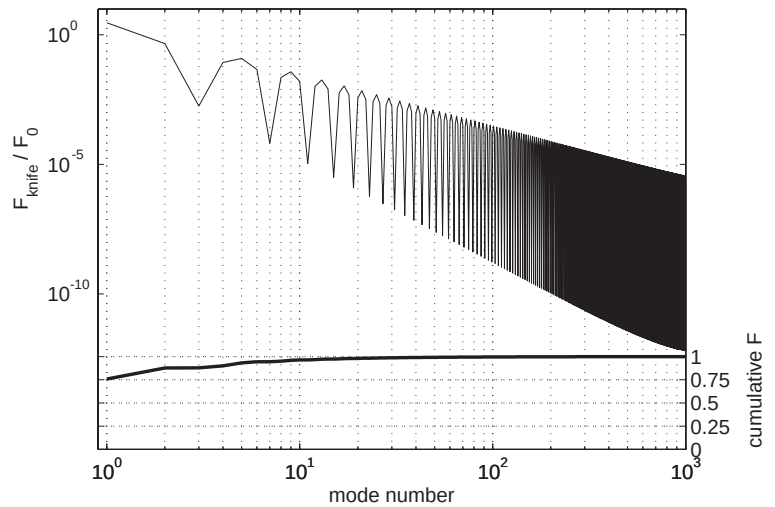

Fig. 3. Nondimensional energy flux for 1000 modes generated from the knife ridge with $\delta = 0.75$. In the lower portion of the panel, the cumulative sum of the energy flux is shown, normalized by the total sum in (21).

$a_n = A_{mn}^{-1} c_m$. In general, only O(300) terms of the series expansions are needed to give solutions that comply within 1% of the matching conditions (8)–(11). The higher mode contributions become important when $\delta \to 1$. Fig. 2 shows the horizontal velocity field (u_1 and u_2) for the case of $\delta = 0.75$. The rays emanating from the critical generation point at the ridge tip are clearly visible. For the constant stratification used in this calculation, the wave energy is concentrated along the characteristic linear paths given by $\mathrm{d}x/\mathrm{d}z = \pm\alpha^{-1}$. The current amplitudes along the upward and downward paths are equal.

For this finite depth system, the conversion rate is equal to the energy flux away from the topography. The depth-integrated energy flux is given by

$$F_{\text{knife}} = \int_{-H}^{0} \langle p'u' \rangle \, \mathrm{d}z = F_0 \sum_{n=1}^{\infty} n^{-1} a_n^2, \tag{21}$$

where F_0 is given by (4) and $\langle \cdot \rangle$ denotes an average over all components of wave phase. Fig. 3 shows the nondimensional energy flux for 1000 modes for the case of $\delta = 0.75$. The spectrum is

red, with the energy flux in mode 1 accounting for 75% of the total sum in (21).

We can compare (21) to the linear theory solution for baroclinic energy flux caused by tidal flow over a two-dimensional ridge of varying steepness. Specifically, we examine a topographic ridge with the "Witch of Agnesi" profile, $h(x) = h_0(1 + (x^2/b^2))^{-1}$ (the story behind the name of this curve is given in Chapter 3 of Singh (1997)). Bell (1975) examined the internal tide generation by this in an infinitely deep ocean, and Llewellyn Smith and Young (2002) examined the modal response to wave generation in an ocean of finite depth. Using their formulation, it is possible to express the conversion rate for the witch as

$$F_{\text{witch}} = F_0 \frac{\pi^2}{4} \delta^2 \sum_{n=1}^{\infty} nc^2 e^{-nc} = F_0 \frac{\pi^2}{4} \delta^2 \frac{c^2 e^{-c}}{(1 - e^{-c})^2}, \quad (22)$$

where $c = (3^{3/2}\pi/4)(\delta/\varepsilon)$, and the slope parameter for the maximum topographic steepness is given by

$$\varepsilon = \alpha^{-1} \left(\frac{3^{3/2}}{8} \right) \frac{h_0}{b}. \quad (23)$$

In the limit of $\delta/\varepsilon \ll 1$, (22) reduces to the result for an infinitely deep ocean presented by Bell (1975),

$$F_{\text{witch}} \simeq F_0(\pi^2/4)\delta^2. \quad (24)$$

As discussed by Llewellyn Smith and Young (2002), (24) is independent of the width of the sloping region.

Fig. 4 shows the ratio of F_{knife} from (21) to F_{witch} from (22) for the case of a witch ridge with critical slope, $\varepsilon = 1$. Here, we have stretched the applicability of the linear theory estimate, since (22) is formally valid only for $\varepsilon \ll 1$. However, this estimate for critical generation provides the basis for a useful comparison with (21). In the limit of $\delta \ll 1$, the knife produces twice the energy flux predicted for the witch. Specifically, we find $F_{\text{knife}}/F_{\text{witch}}$ is equal to 2.000 ± 0.0004 for 10 calculations in the parameter range $0.003 < \delta < 0.03$. Thus, it seems that $F_{\text{knife}}/F_{\text{witch}}$ is exactly 2 for $\delta \ll 1$, as Llewellyn Smith and Young (in press) have now found analytically. Since (24) is

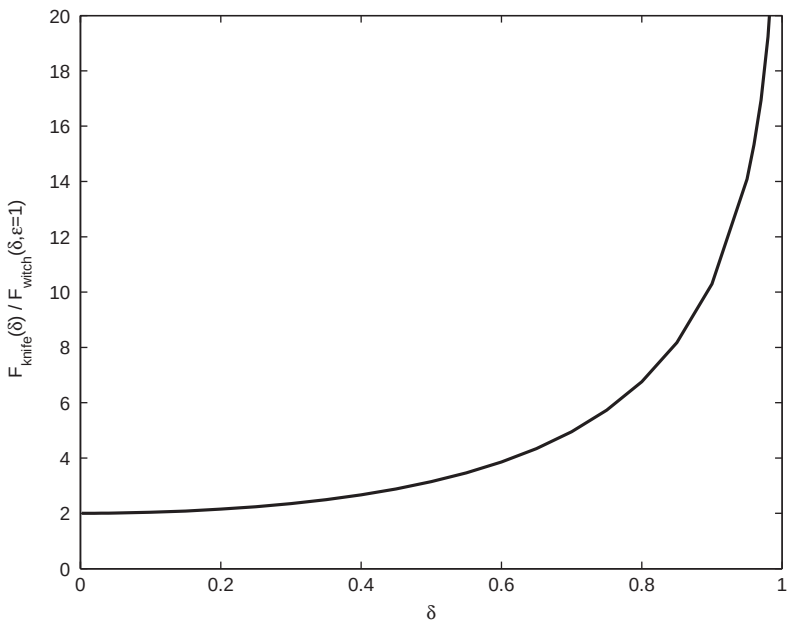

Fig. 4. Ratio of the knife-edge ridge energy flux to the linear theory estimate of energy flux for a Witch of Agnesi ridge. The witch energy flux was computed from (22), with $\varepsilon = 1$.

independent of ε, this result is generally applicable to the linear theory solution for witch topography with $\delta \ll 1$ of arbitrary steepness.

The energy flux production from the knife exceeds the linear prediction by more than a factor of 4 for $\delta > 0.6$ (Fig. 4).

3. Internal tide generation at a step

We now consider a topographic step at $x = 0$, where the depth is $-H$ on the deep side of the step and $-H + h_0$ on the shallow side of the step (Fig. 5). A barotropic tidal current given by $U(t) = U_0 \cos \omega t$ is taken perpendicular to the barrier. This problem was examined by Stigebrandt (1980), who assumed that the wave response occurred only on the deep side of the step. We allow internal tides to radiate away from the step in both directions. In this case, the modal solutions take the form:

$$u_1 = U_0 \sum_{n=1}^{\infty} a_n \cos\left(\frac{n\pi z}{H}\right) \cos(k_n x + \omega t),$$

$$u_2 = U_0 \sum_{n=1}^{\infty} b_n \cos\left(\frac{n\pi z}{H - h_0}\right) \cos(-k_n' x + \omega t), \tag{25}$$

$$w_1 = \alpha U_0 \sum_{n=1}^{\infty} a_n \sin\left(\frac{n\pi z}{H}\right) \sin(k_n x + \omega t),$$

$$w_2 = -\alpha U_0 \sum_{n=1}^{\infty} b_n \sin\left(\frac{n\pi z}{H - h_0}\right) \times \sin(-k_n' x + \omega t). \tag{26}$$

Here, (u_1, w_1) are the baroclinic velocity components on the deep side ($x < 0$) of the step where the horizontal and vertical wavenumbers are given by $k_n = \alpha n\pi/H$ and $n\pi/H$, respectively. The velocity components on the shallow side ($x > 0$) of the step are (u_2, w_2), with wavenumbers $k_n' = \alpha n\pi/(H - h_0)$ and $n\pi/(H - h_0)$. The matching conditions at $x = 0$ are similar to (8)–(10), with the barotropic velocity on the shallow side of the step scaled by $H/(H - h_0)$. These can be stated as

$$\sum_{n=1}^{\infty} a_n \sin\frac{n\pi z}{H} = \sum_{n=1}^{\infty} b_n \sin\frac{n\pi z}{(H - h_0)}, \quad -H + h_0 \leqslant z \leqslant 0, \tag{27}$$

$$1 + \sum_{n=1}^{\infty} a_n \cos\frac{n\pi z}{H} = \frac{H}{(H - h_0)} + \sum_{n=1}^{\infty} b_n \cos\frac{n\pi z}{(H - h_0)}, \quad -H + h_0 \leqslant z \leqslant 0, \tag{28}$$

$$1 + \sum_{n=1}^{\infty} a_n \cos\frac{n\pi z}{H} = 0, \quad -H \leqslant z < -H + h_0. \tag{29}$$

The terms in (28) and (29) can be multiplied by $\cos m\pi z/H$ and integrated vertically. For $n = 1, \ldots, N$ modes and $m = 1, \ldots, N$, this gives a coupled set of equations for the coefficients a_m and b_n which can be written as the matrix problem:

$$a_m = A_{mn} b_n + c_m. \tag{30}$$

Additionally, multiplying the terms in (27) by $\sin l\pi z/(H - h_0)$ and vertically integrating the set of equations generated by taking $l = 1, \ldots, N$ gives the matrix problem:

$$b_n = B_{nl} a_l. \tag{31}$$

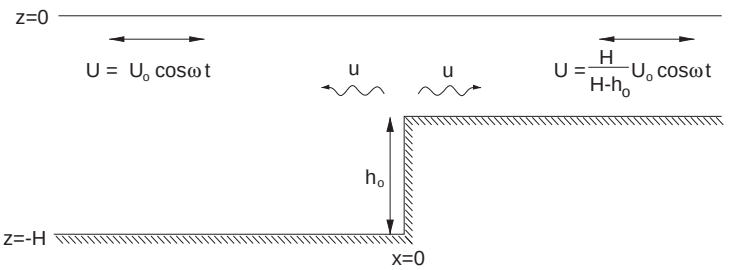

Fig. 5. Sketch showing a topographic step of height h_0 above a deep ocean of depth H. The barotropic tidal current and baroclinic response are denoted by U and u, respectively.

The matrices for the two coupled problems are given by

$$A_{mn} = \frac{2m(1-\delta)^2(-1)^n \sin m\pi(1-\delta)}{\pi[m^2(1-\delta)^2 - n^2]}, \tag{32}$$

$$B_{nl} = \frac{2n(-1)^n \sin l\pi(1-\delta)}{\pi[n^2 - l^2(1-\delta)^2]}, \tag{33}$$

$$c_m = \frac{2\sin m\pi(1-\delta)}{m\pi(1-\delta)}. \tag{34}$$

The coefficients for the baroclinic velocity series are solved by combining (30) and (31) into a single matrix inversion,

$$a_l = (I - A_{mn}B_{nl})^{-1}c_m, \tag{35}$$

where I is the identity matrix. Using (31) and (35), the modal coefficients were computed for 2000 baroclinic modes. Fig. 6 shows the horizontal velocity field (u_1 and u_2) for the case of $\delta = 0.75$. The amplitudes of the baroclinic velocities are largest along characteristic paths, with slope $dx/dz = \pm\alpha^{-1}$ emanating from the edge of the step. On the deep-side of the step, the current amplitudes along the upward and downward paths are equal.

The depth-integrated energy flux is given by

$$F_{\text{step}} = \int_{-H}^{0} \langle p'u' \rangle \, dz = \frac{1}{2}F_0 \sum_{n=1}^{\infty} n^{-1}[a_n^2 + (1-\delta)^2 b_n^2], \tag{36}$$

where $\langle \cdot \rangle$ denotes an average over all components of wave phase. Fig. 7 shows the nondimensional energy flux for 1000 modes for the case of $\delta = 0.75$. As in the case of the knife-edge spectrum, the step spectrum is red with mode 1 accounting for 75% of the total sum in (36). Fig. 8 shows the fraction of energy flux radiated to the shallow side of the step relative to the total flux. In the limit of infinitesimal topography, the energy flux radiated to each side is equal, as expected from symmetry. However, the energy flux radiated to the shallow side of the step drops to less than 10% for $\delta \geqslant 0.25$. The asymptotic behavior of (36) as $\delta \to 0$ can be derived through analysis of terms in (32)–(34) and the use of (30) and (31). It can be shown that for modes with $n < O(\delta^{-1})$,

$$\lim_{\delta\to 0} a_n = -\lim_{\delta\to 0} b_n = -(-1)^n\delta, \tag{37}$$

which implies

$$\lim_{\delta\to 0} F_{\text{step}} = F_0\delta^2 \sum_{n=0}^{O(\delta^{-1})} n^{-1} = F_0\delta^2 \ln(a\delta^{-1}) + \text{smaller terms}. \tag{38}$$

The leading term in (38) provides an excellent approximation to F_{step} in the limit of small δ when $a \simeq 3.4$. We compare (36) to the linear theory solution for energy flux by tidal flow over a two-dimensional slope up to a shelf. Specifically, we will examine a topographic slope with the profile $h(x) = \pi^{-1}h_0 \tan^{-1}(x/b)$. We note that this

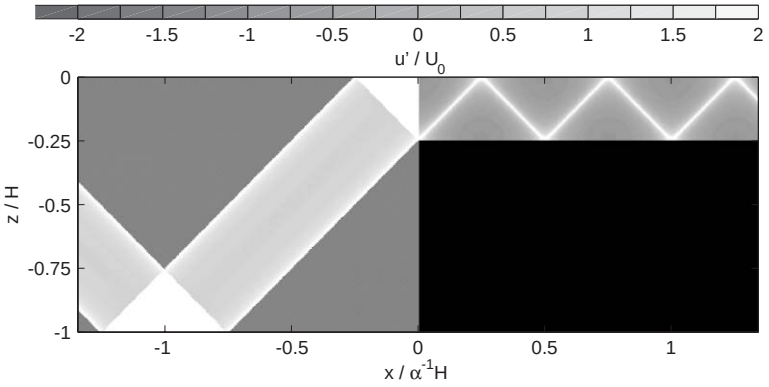

Fig. 6. A snapshot of instantaneous baroclinic velocity (u_1 and u_2 at $\omega t = 0, 2\pi, 4\pi, \ldots$, from (25)), normalized by the barotropic current amplitude, for a topographic step with $\delta = 0.75$. Dark gray shading on the deep side of the step indicates regions where $u = -U_0$.

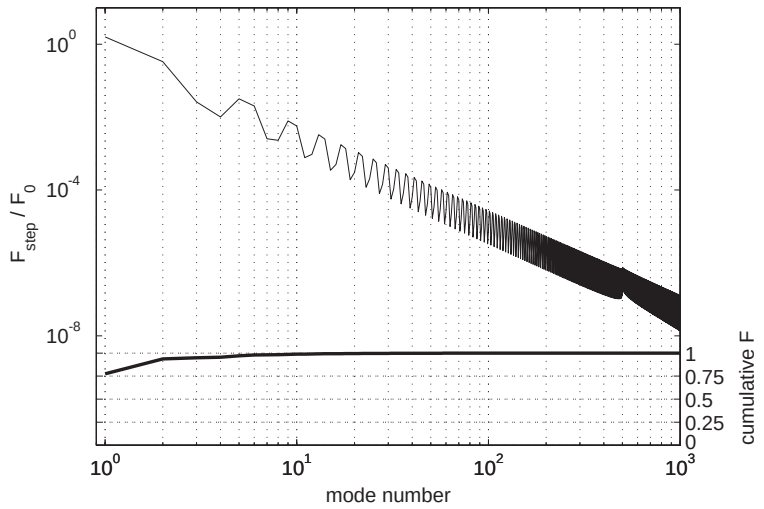

Fig. 7. Nondimensional energy flux for 1000 modes generated from the step with $\delta = 0.75$. In the lower portion of the panel, the cumulative sum of the energy flux is shown, normalized by the total sum in (36).

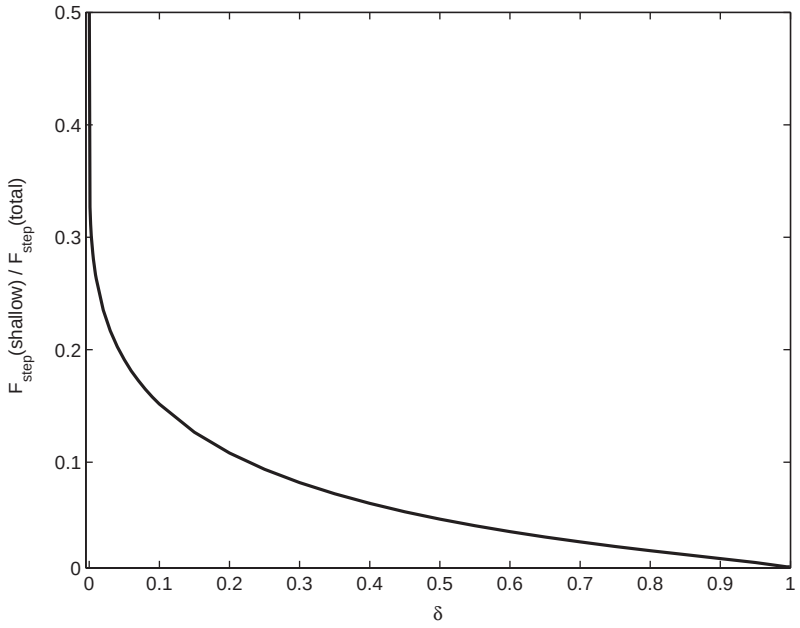

Fig. 8. Fraction of energy flux radiated to the shallow side of the step relative to the total flux.

arctan slope is related to the spatial derivative of the Witch of Agnesi profile, just as the step relates to the knife-edge. The linear conversion rate for this slope can be calculated using the theory of Llewellyn Smith and Young (2002) as

$$F_{\text{slope}} = F_0\delta^2 \sum_{n=1}^{\infty} n^{-1} e^{-4n\delta/\varepsilon(2-\delta)} = -F_0\delta^2 \ln(1 - e^{-4\delta/\varepsilon(2-\delta)}), \quad (39)$$

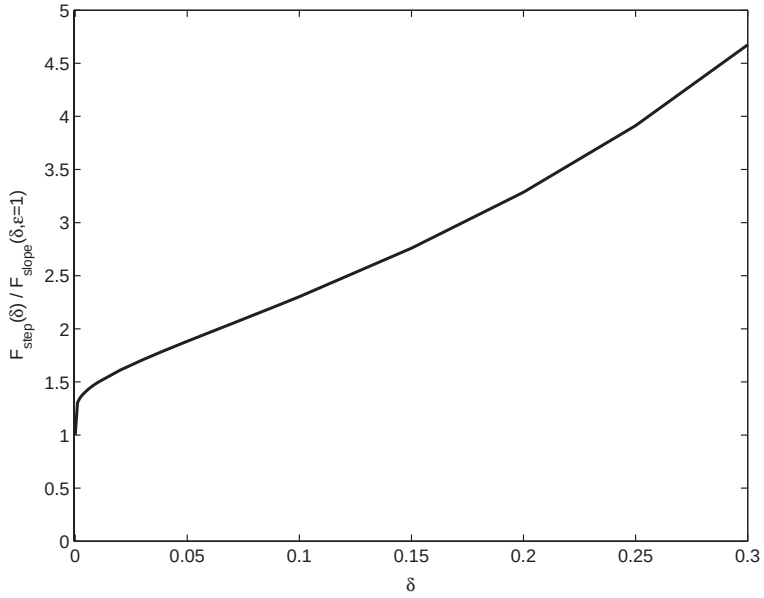

Fig. 9. Ratio of step generated energy flux to the linear theory estimate of energy flux for a slope.

where the slope parameter for the maximum topographic steepness is given by

$$\varepsilon = \alpha^{-1}\pi^{-1}\frac{h_0}{b}. \tag{40}$$

In the limit of $\delta/\varepsilon \ll 1$, the conversion rate is approximated by

$$F_{\text{slope}} \simeq -F_0\delta^2 \ln\left(\left[\frac{2-\delta}{4}\right]\frac{\varepsilon}{\delta}\right). \tag{41}$$

Furthermore, if both $\delta \ll 1$ and $\delta/\varepsilon \ll 1$,

$$F_{\text{slope}} \simeq F_0\delta^2 \ln(\tfrac{1}{2}\varepsilon/\delta), \tag{42}$$

which to lowest order in δ is the same as (38) for the step energy flux. Unlike the case of $\delta \ll 1$ and $\delta/\varepsilon \ll 1$ for a ridge as in (24), (42) remains dependent on ε/δ, and hence the width of the sloping region, even in the limit of an infinitely deep ocean.

Fig. 9 shows the ratio of F_{step} to F_{slope} for the case of a critical slope. In the limit of $\delta \ll 1$, the step and the slope produce the same energy flux, as expected from (38) and (42). However, this ratio increases rapidly as δ is increased, with $F_{\text{step}}/F_{\text{slope}} \simeq 1.3$ for $\delta = 0.001$. Normalizing F_{step} by F_{slope} with $\varepsilon = 6.8$ produces a curve that approaches unity smoothly in the limit of $\delta = 0$. The energy flux from the topographic step exceeds the linear prediction by more than a factor of 4 for $\delta > 0.3$.

4. Internal tide generation at topography of finite width

4.1. A top-hat ridge

The formulation and solution technique for the step is readily adapted to the problem of internal tide generation by a top hat, rather than knife-edge ridge. As shown in Fig. 10, we still consider a ridge of height h_0 in an ocean of depth H, but now give it a width $2L$. The barotropic tide is, as before, $U_0 \cos \omega t$ in regions 1 and 3, and $H/(H-h_0)$ times this in region 2. The baroclinic part of the solution in regions 1 and 3 is now composed of internal modes propagating away from the ridge, but in region 2 the baroclinic solution must be standing waves. Symmetry conditions require that $w = 0$ at $x = 0$, so that we may write the baroclinic

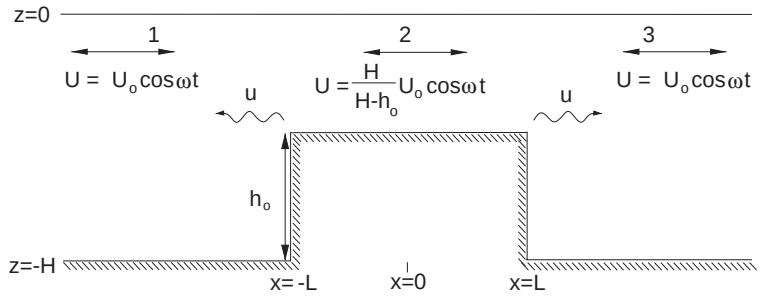

Fig. 10. Schematic of a top-hat ridge of height h_0 and width $2L$.

solution in regions 1 and 2 as

$$u_1 = \mathrm{Re}\left\{ U_0 \sum_{n=1}^{\infty} a_n \cos\left(\frac{n\pi z}{H}\right) e^{i(k_n x+\omega t)} \right\},$$

$$u_2 = \mathrm{Re}\left\{ U_0 \sum_{n=1}^{\infty} b_n \cos\left(\frac{n\pi z}{H-h_0}\right) \cos k_n' x e^{i\omega t} \right\}, \quad (43)$$

$$w_1 = \mathrm{Re}\left\{ -i\alpha U_0 \sum_{n=1}^{\infty} a_n \sin\left(\frac{n\pi z}{H}\right) e^{i(k_n x+\omega t)} \right\},$$

$$w_2 = \mathrm{Re}\left\{ \alpha U_0 \sum_{n=1}^{\infty} b_n \sin\left(\frac{n\pi z}{H-h_0}\right) \sin k_n' x e^{i\omega t} \right\}. \quad (44)$$

The solution in region 3 is as in region 1 with a change of sign in k_n and w. As for the step, the total horizontal velocity must match across $x = -L$ for $-H+h_0<z<0$ and be zero for $-H<z<-H+h_0$, and w must also be continuous at $x=-L$ for $-H+h_0<z<0$. As for the step, this leads to two coupled matrix equations for the coefficients a_n and b_n, though these coefficients may now be complex. Because of the symmetry of the problem, the matching conditions at $x=\pm L$ lead to exactly the same matrix equations as for the step. However the total energy flux away from the ridge is now given by $F_0 \sum_{n=1}^{\infty} n^{-1}|a_n|^2$. We proceed much as before by solving the problem for 2000 modes for a variety of values of the ratio $\delta = h_0/H$ and for various values of the width parameter $\xi = \alpha\pi L/H$.

Fig. 11 shows the internal tide energy flux radiated from the top-hat ridge compared with that from the knife edge, as a function of ξ and for various values of the depth ratio $\delta = h_0/H$. As required, the energy flux ratio tends to 1 for an infinitely narrow ridge with $\xi = 0$. It is also easily seen from the structure of the problem that the solution is periodic in ξ, with a period of 2π. The energy flux is, in fact, periodic with a period of π and symmetric about $\xi = \pi/2$. It may seem a bit physically surprising that for $\xi = \pi$, or any integer multiple of this, the radiated energy is the same as from a knife edge, but the most interesting result is the weak dependence of the flux on the depth ratio δ. Even for δ as small as 0.1, the maximum increase in energy flux, over that for the knife edge, is only about 70%, and is much less for a ridge that occupies a significant fraction of the water column. The knife edge thus seems to be a good model for many tall ridges in the ocean. For very small values of δ, the internal tide is as for two steps. However, if ξ is an integer multiple of π, the waves generated at each edge of the ridge destructively interfere. For ξ well away from multiples of π, and given the asymptotic fluxes (24) and (38), the energy flux is much greater than for a knife edge of the same height.

4.2. A top-hat trench

It is also straightforward to extend the above problem to a trench of depth h_0 in an ocean of depth H elsewhere (Fig. 12). The energy flux clearly vanishes for $\xi = 0$ at which the trench has collapsed to zero width. Interestingly, as a consequence of the periodicity of the problem, this result of zero flux also applies if ξ is an integer

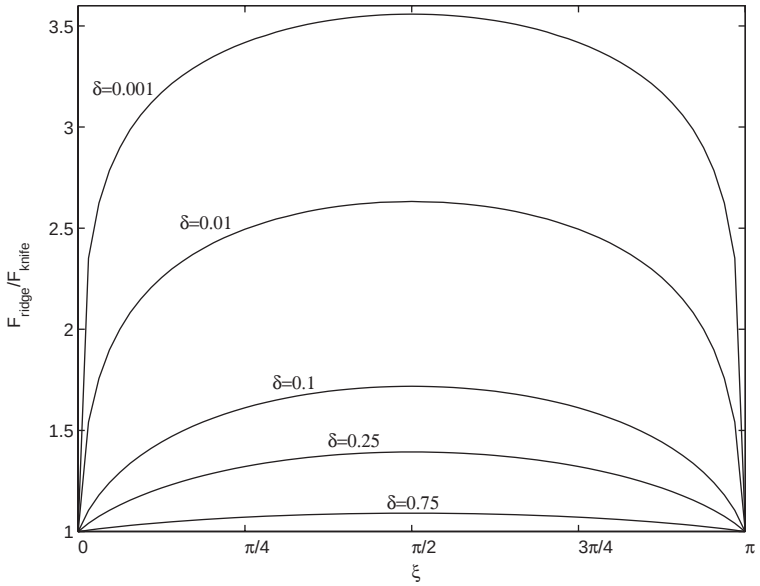

Fig. 11. Energy flux generated by the top-hat ridge normalized by the energy flux generated by the knife-edge ridge. The nondimensional ridge width parameter is given by $\xi = \alpha\pi L/H$.

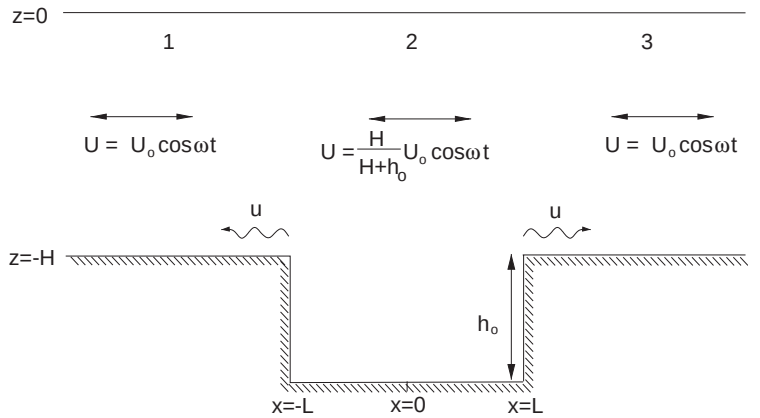

Fig. 12. Sketch showing a top-hat trench of depth h_0 (relative to $z = -H$) and width $2L$.

multiple of π. Fig. 13 shows the energy flux for a trench compared with that for a ridge of the same width as a function of the ratio $\delta = h_0/H$, where h_0 is the depth of the trench or height of the ridge relative to $z = -H$. For small values of δ the trench, like the ridge, generates internal tides as from two steps. For ξ away from integer multiples of π, the energy flux from the trench is almost the same as from the ridge. As δ increases, the range in ξ of this near equality is reduced and only holds exactly at $\xi = \pi/2$. The results show that for a trench, unlike the situation for a ridge, the energy flux generated is a rather sensitive function of the width.

5. Discussion

5.1. The Hawaiian Ridge

Our model of internal tide generation at a knife-edge ridge can serve as a crude model for internal

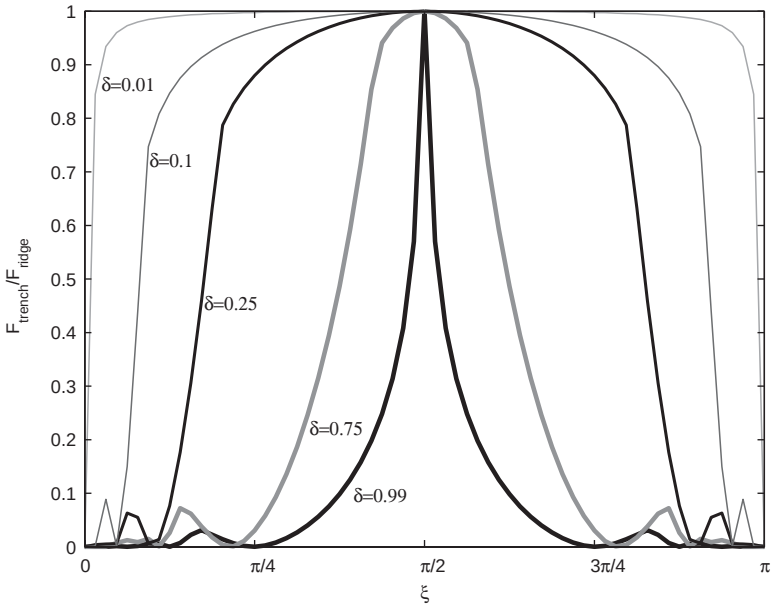

Fig. 13. Energy flux generated by the top-hat trench normalized by the energy flux generated by the top-hat ridge of equal height amplitude.

tide generation at the Hawaiian Ridge, or other tall ridges. The Hawaiian Ridge has been the focus of numerous internal tide studies (Ray and Mitchum, 1996, 1997; Kang et al., 2000; Pinkel et al., 2000; Merrifield et al., 2001), and Althaus et al. (in press) have observed internal tides from the knife-edge like Mendocino Escarpment. Here, we approximate the Hawaiian Ridge as a knife-edge ridge with $\delta = 0.75$ ($h_0 = 3000$ m and $H = 4000$ m). The nondimensional energy flux spectrum for this case is shown in Fig. 3. We now seek a dimensional estimate of the energy flux. We use $N = 5 \times 10^{-3}$ s^{-1} as a rough scale for the stratification at 1000 m depth, near the critical generation point on the ridge. We take other parameters as $\omega = 1.4 \times 10^{-4}$ s^{-1}, $f = 5 \times 10^{-5}$ s^{-1}, and $U_0 = 0.02$ m s^{-1} to estimate $F_{\text{knife}} = 11,000$ W m^{-1}. Taking 2000 km as the Hawaiian Ridge length, this implies 21 GW of M_2 internal tide production. This estimate is close to the 20 GW estimated by Egbert and Ray (2000, 2001) for the total barotropic tidal conversion occurring at Hawaii, but larger than the model result by Merrifield et al. (2001) of 9 GW for the energy flux radiated away from the ridge. We note that our parameter values are somewhat subjective. The depth of the Hawaiian Ridge cannot realistically be characterized by a single value of δ. Also, the barotropic current amplitude varies significantly over the Hawaiian Ridge, and a 40% change in the value of U_0 results in a factor of two change in F_{knife}. Additionally, if WKB stretching of depth is considered to account for varying stratification with depth, a more appropriate value of δ is given by the ratio of stretched variables, $\delta_{\text{WKB}} = (\hat{H} - (\widehat{H - h_0}))/\hat{H}$, where $\hat{z} \cong \int_z^0 (N(z')/N_{\text{ref}})\,\mathrm{d}z'$ (Leaman and Sanford 1975). Here, N_{ref} is a reference value of the stratification, which may be taken as the stratification value at the ridge crest where the critical internal tide generation occurs. Using an exponential stratification, $N(z) = N_0 e^{z/b}$ with $N_0 = 0.00524$ s^{-1} and $b = 1300$ m, we estimate $\delta_{\text{WKB}} = 0.44$ for the Hawaiian Ridge. With $U_0 = 0.02$ m s^{-1}, this implies $F_{\text{knife}} = 3000$ W m^{-1}, or roughly 6 GW summed around the ridge.

While the total energy flux is sensitive to the choice of parameters, the ratio of the mode-1 energy flux to the total energy flux is not. Fig. 14 shows this ratio for general δ. For the case of $\delta = 0.75$, mode 1 carries roughly 75% of the total flux. Ray and Mitchum (1997) have used sea-surface

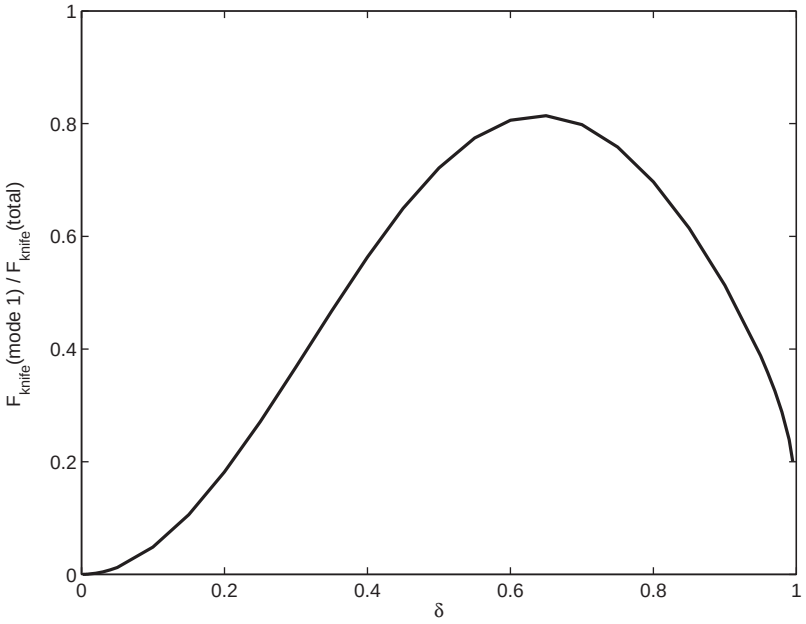

Fig. 14. Ratio of mode-1 energy flux to the total energy flux for a knife-edge ridge.

altimetry data to estimate that 15 GW of mode-1 internal tide energy is radiated by the Hawaiian Ridge. This is indeed 75% of the Egbert and Ray (2000, 2001) estimate for the total internal-tide energy flux. We note that a knife-edge ridge of height $\delta = 0.65$ generates a mode-1 baroclinic response containing roughly 80% of the total flux.

5.2. Internal tide generation at multiple steps

Following Stigebrandt (1980), several studies have applied the result for internal tide generation at a single step to arrangements of multiple steps (Sjöberg and Stigebrandt, 1992; Gustafsson, 2001). These models attempt to represent arbitrary topography as a series of vertical pillars, with internal tide generation occurring at the steps between them. Stigebrandt (1980) assumed that internal tide energy was radiated to the deep ocean side of the step only. He applied this simplification in fjords where the radiation of the internal tide onto a shallow sill was assumed to be negligible. However, Sjöberg and Stigebrandt (1992) and Gustafsson (2001) apply this simplification to topographic steps in the deep ocean where the deep and shallow sides of the step are of similar depth. Furthermore, these studies treat each topographic step as an independent generator of internal tides, ignoring the interference between internal tides produced at two or more nearby steps. This simplification is clearly applicable to fjords, where one topographic step is used to represent a sill. However, multiple steps are needed to represent general topography in the deep ocean, and the neglect of interference phenomena makes the usefulness of the resulting estimates questionable.

We have examined the Sjöberg and Stigebrandt (1992) energy flux estimate for the Witch of Agnesi topography. As discussed previously, the linear theory conversion rate for the witch is given by (22). Here, we will focus on the limit of $\delta/\varepsilon \ll 1$, with $F_{\text{witch}} = F_0(\pi^2/4)\delta^2$. The witch topography can be represented as a series of vertical pillars, and Sjöberg and Stigebrandt (1992) estimate the internal tide energy flux from each pillar as

$$F_{\text{pillar}} = 2F_0 \sum_{j=1}^{\infty} j^{-1} \frac{\sin^2(j\pi[1-\delta])}{\pi^2 j^2 (1-\delta)^2}, \tag{45}$$

where the sum is over modes with index j. For each pillar, δ is taken as the difference in height from the neighboring pillar normalized by the water

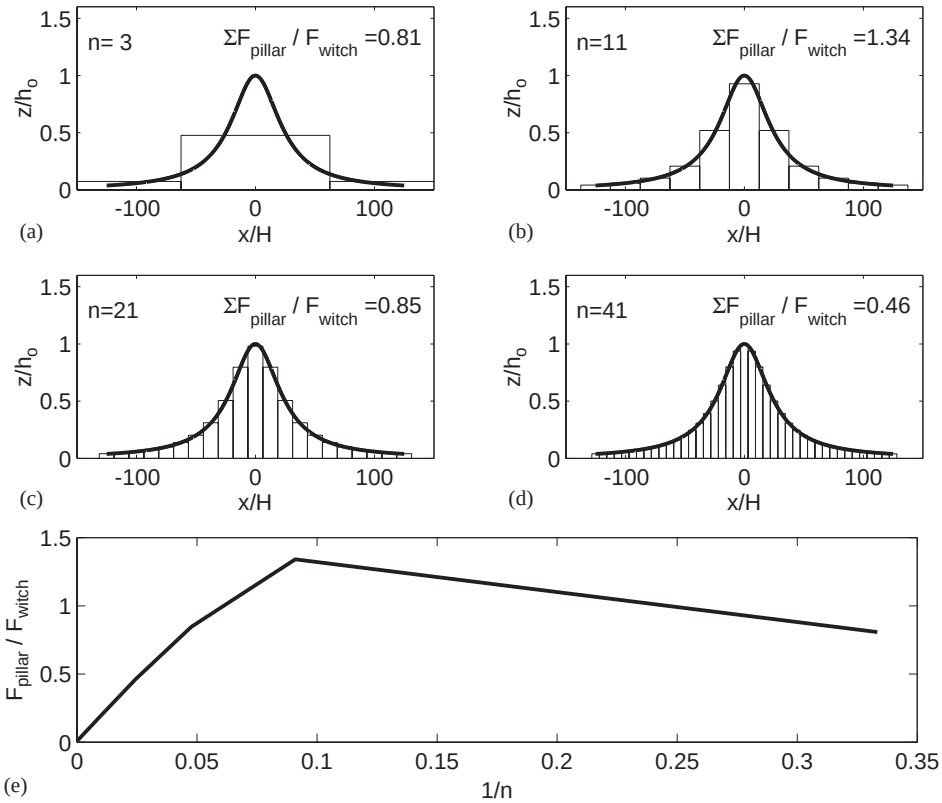

Fig. 15. Calculations using the pillar model of Sjöberg and Stigebrandt (1992), applied to the Witch of Agnesi ridge. Panels a–d show successively increasing pillar representations of the same topography. The number of pillars (n) is reported in the upper left corner of each panel, and the total pillar energy flux to the witch-topography energy flux is shown in the upper right. Panel e shows the energy flux ratio for pillar representations with $n = 3$–5000.

depth above the pillar. In the case where the difference in height between pillars is small compared to the total depth ($\delta \ll 1$), (45) can be expressed as

$$F_{\text{pillar}} = 2F_0\delta^2 \sum_{j=1}^{\mathrm{O}(\delta^{-1})} j^{-1}(1 + \mathrm{O}(2\delta)). \tag{46}$$

Here, the approximation is valid out to $j \simeq \mathrm{O}(\delta^{-1})$. Sjöberg and Stigebrandt (1992) and Gustafsson (2001) truncate the summation in (45) at mode 10. The total energy-flux (per unit cross-stream width) $\sum F_{\text{pillar}}$ is calculated by summing the conversion rates of all the pillars.

Fig. 15 shows the Witch of Agnesi topography represented as a series of vertical pillars. Four different representations of the witch are shown for an increasing number of pillars (n). In each case, (45) was used to estimate the energy flux for each pillar. The ratio $\sum F_{\text{pillar}}/F_{\text{witch}}$ is reported in upper right of each panel. The witch is coarsely resolved by 3 pillars in panel a, and panels b–d show successively more numerous pillars with smaller steps which resolve the topography with increased accuracy. The general trend is that $\sum F_{\text{pillar}}$ approaches zero linearly as the number of steps is increased (panel e). We note that Sjöberg and Stigebrandt (1992) and Gustafsson (2001) represent an obstacle's total height (h_0) with n steps, such that δ for each pillar is $H^{-1}(h_0/n)$. It follows from (46) that

$$\sum F_{\text{pillar}} \propto n \times H^{-2}\frac{h_0^2}{n^2}\ln n. \tag{47}$$

Since Sjöberg and Stigebrandt (1992) and Gustafsson (2001) truncate the summation at $j = 10$, their energy flux estimates are proportional to n^{-1} rather than $n^{-1} \ln n$. Fig. 15e confirms that $\sum F_{\text{pillar}} \propto n^{-1}$, causing the energy flux estimate to approach zero as the number of pillars becomes large. This is a general problem, not related to truncating the sum in (46), and not limited to any specific topographic shape.

Thus, in cases where a series of steps are needed to represent topography, the estimates of Sjöberg and Stigebrandt (1992) and Gustafsson (2001) will be sensitive to the number of steps used to resolve the bathymetry. While the energy flux estimates presented in these studies are plausible, their results must be viewed as fortuitous. A valid model for internal tide generation at a series of steps must include interference phenomena occurring between internal tides generated at neighboring steps. Interference effects allow for convergence of internal tide estimates as the number of steps is increased to better resolve the topography.

6. Conclusion

A knife-edge ridge may be regarded as a simple model for an isolated ridge of supercritical steepness such as Hawaii. We have found that in the limit of infinitesimal amplitude topography, a knife-edge ridge produces exactly twice the amount of energy flux as the linear prediction for critical topography. We contrast this to the estimate of Balmforth et al. (2002) for a gaussian ridge. They find that at critical steepness, the energy flux produced by the ridge is 1.14 times greater than the linear prediction. Generalizing, we conclude that in the infinitesimal topography limit ($\delta \ll 1$), increasing the steepness from $\varepsilon = 1$ to $\varepsilon = \infty$ increases the power production by only a further 75%. However, we note that for a knife-edge ridge of finite amplitude, the energy flux can considerably exceed the linear theory estimates. We have further found that the knife-edge ridge is an efficient generator for the first baroclinic mode. For $0.35 < \delta < 0.9$, mode-1 accounts for 50% or more of the total energy flux. It seems likely that for large amplitude ridges such as Hawaii, the internal tide energy flux is largely determined by the overall topographic height, and not by finer scale roughness along the ridge. This contrasts the internal tide generation occurring at mid-ocean ridges, where the energy flux is produced by roughness at all scales (e.g., St. Laurent and Garrett, 2002).

The case of a topographic step was also considered. In the limit of infinitesimal topography, the energy flux of the step equals the linear theory prediction for a slope of critical steepness. Energy flux estimates for step topography have been previously employed in calculations by Sjöberg and Stigebrandt (1992) and Gustafsson (2001). In those studies, deep ocean topography was represented as pillars of varying height, and estimates of internal tide energy flux were made at the steps between adjacent pillars. Since Sjöberg and Stigebrandt (1992) and Gustafsson (2001) regard each step as an independent generator of the tides, their estimates are entirely dependent on the number of pillars used to represent the topography. In the limit of many pillars for which the topography is finely resolved, the Sjöberg and Stigebrandt (1992) and Gustafsson (2001) calculations predict a vanishing energy flux.

For the case of mid-ocean ridges such as the Mid Atlantic Ridge, changes in depth over the lateral scale of the mode-1 tidal wavelength (O(150 km)) are generally less than 500 m. This provides a rough estimate for the height h_0 of topographic obstacles along the mid-ocean ridge. Furthermore, the mean depth H of a mid-ocean ridge system can vary from 3000 to 5000 m. Thus, $0.1 < \delta < 0.2$ is a rough estimate of the amplitude range for typical mid-ocean ridge topographies. These regions are also characterized as subcritical (St. Laurent and Garrett, 2002). It therefore seems reasonable to use linear theory for the internal tides generated at mid-ocean ridge topographies. The complex topography at these sites can then be modeled as individual Fourier components, and the total baroclinic response is determined through superposition. The simple models for knife-edge, step, and top-hat topography are not useful for calculating internal tide energy flux at these sites. Additionally, the methods of Sjöberg and

Stigebrandt (1992) and Gustafsson (2001) will not produce reliable estimates of energy flux for mid-ocean ridge regions.

In contrast, ridges associated with oceanic island and trench systems, such as the Hawaiian and Aleutian Ridges, are both large amplitude ($0.5 < \delta < 1$) and supercritical. Linear theory for the internal tides will significantly under-estimate the energy flux produced at these topographies. We propose that the simple model for the knife-edge ridge can serve as the basis for energy flux estimates for these features.

Acknowledgements

The authors acknowledge the support of the US Office of Naval Research and the Natural Science and Engineering Council of Canada. DP-J thanks NSERC for an Undergraduate Student Research Award. We thank Eric Kunze, and three anonymous reviewers for helpful comments.

References

Althaus, A.M., Kunze, E., Sanford, T.B. Internal tide radiation from Mendocino Escarpment. Journal of Physical Oceanography, in press.

Baines, P.G., 1973. The generation of internal tides by flat-bump topography. Deep-Sea Research 20, 179–205.

Baines, P.G., 1982. On internal tide generation models. Deep-Sea Research 29, 307–338.

Balmforth, N.J., Ierley, G.R., Young, W.R., 2002. Tidal conversion by nearly critical topography. Journal of Physical Oceanography 32, 2900–2914.

Bell, T.H., 1975. Lee waves in stratified flows with simple harmonic time dependence. Journal of Fluid Mechanics 67, 705–722.

Cox, C.S., Sandstrom, H., 1962. Coupling of surface and internal waves in water of variable depth. Journal of the Oceanographic Society of Japan 20th Anniversary Volume, 499–513.

Craig, P.D., 1987. Solutions for internal tide generation over coastal topography. Journal of Marine Research 45, 83–105.

Egbert, G.D., Ray, R.D., 2000. Significant dissipation of tidal energy in the deep ocean inferred from satellite altimeter data. Nature 405, 775–778.

Egbert, G.D., Ray, R.D., 2001. Estimates of M_2 tidal energy dissipation from TOPEX/POSEIDON altimeter data. Journal of Geophysical Research 106, 22475–22502.

Gustafsson, K.E., 2001. Computations of the energy flux to mixing processes via baroclinic wave drag on barotropic tides. Deep-Sea Research 48, 2283–2295.

Hibiya, T., 1986. Generation mechanism of internal waves by tidal flow over a sill. Journal of Geophysical Research 91, 7696–7708.

Kang, S.K., Foreman, M.G.G., Crawford, W.R., Cherniawsky, J.Y., 2000. Numerical modeling of internal tide generation along the Hawaiian Ridge. Journal of Physical Oceanography 30, 1083–1098.

Khatiwala, S., 2003. Generation of internal tides in the ocean. Deep-Sea Research I 50, 3–21.

Larsen, L.H., 1969. Internal waves incident upon a knife edge barrier. Deep-Sea Research 16, 411–419.

Leaman, K.D., Sanford, T.B., 1975. Vertical energy propagation of inertial waves: a vector spectral analysis of velocity profiles. Journal of Geophysical Research 80, 1975–1978.

Li, M. Energetics of internal tides radiated from deep-ocean topographic features. Journal of Physical Oceanography, submitted for publication.

Llewellyn Smith, S.G., Young, W.R. 2002. Conversion of the barotropic tide. Journal of Physical Oceanography 32, 1554–1566.

Llewellyn Smith, S.G., Young, W.R. Tidal conversion by a very steep ridge. Journal of Fluid Mechanics, submitted for publication.

Merrifield, M.A., Holloway, P.E., Shaun Johnston, T.M., 2001. The generation of internal tides at the Hawaiian Ridge. Geophysical Research Letters 28, 559–562.

Pinkel, R., Munk, W., Worcester, P., et al., 2000. Ocean mixing studied near Hawaiian Ridge. EOS, Transactions of the American Geophysical Union, 81, pp. 545, 553.

Rattray, M., 1960. On the coastal generation of internal tides. Tellus 12, 54–61.

Ray, R., Mitchum, G.T., 1996. Surface manifestation of internal tides generated near Hawaii. Geophysical Research Letters 23, 2101–2104.

Ray, R., Mitchum, G.T., 1997. Surface manifestation of internal tides in the deep ocean: observations from altimetry and island gauges. Progress in Oceanography 40, 135–162.

Robinson, R.M., 1969. The effects of a barrier on internal waves. Deep-Sea Research 16, 421–429.

St. Laurent, L., Garrett, C., 2002. The role of internal tides in mixing the deep ocean. Journal of Physical Oceanography 32, 2882–2899.

Singh, S., 1997. Fermat's Enigma: The Quest to Solve the World's Greatest Mathematical Problem. Walker and Co., New York, 288pp.

Sjöberg, B., Stigebrandt, A., 1992. Computations of the geographical distribution of the energy flux to mixing processes via internal tides and the associated vertical circulation in the ocean. Deep-Sea Research 39, 269–291.

Stigebrandt, A., 1980. Some aspects of tidal interaction with Fjord Constrictions. Estuarine and Coastal Marine Science 11, 151–166.